IEEE Access
Multidisciplinary | Rapid Review | Open Access Journal

Received September 25, 2019, accepted October 25, 2019, date of publication November 4, 2019,
date of current version December 18, 2019.

Digital Object Identifier 10.1109/ACCESS.2019.2951133

Transverse-Stress Compensated Methane Sensor Based on Long-Period Grating in Photonic Crystal Fiber

HAI LIU[1,2], YANZENG ZHANG[1], CONG CHEN[1], BINGBING BAI[1], QIYUAN SHAO[1], HAORAN WANG[1], WEN ZHANG[1], CANCAN CHEN[1], AND SHOUFENG TANG[1]

[1]School of Information and Control Engineering, China University of Mining and Technology, Xuzhou 221116, China
[2]Xuzhou Key Laboratory of Artificial Intelligence and Big Date, Xuzhou 221116, China

Corresponding author: Shoufeng Tang (tsf0816@126.com)

This work was supported by in part by the Fundamental Research Funds for the Central Universities, China University of Mining and Technology, under Grant 2018QNA40.

ABSTRACT A high-sensitive and transverse-stress compensated methane sensor based on a photonic crystal fiber long-period grating (PCF-LPG) is proposed. The outermost layer of the PCF consists of six large side-holes, five of which are coated with methane-sensitive compound film to achieve methane measurement. Such side-hole structure is helpful for gas sensitive reaction, but not conducive to avoiding external stress interference. Therefore, the last large hole is plated with silver layer to eliminate the cross-sensitivity effect through adding a Surface Plasmon Resonance (SPR) sensing channel with the consideration of photo-elastic effect and material deformation. Results show that the methane gas sensitivity can reach up to 6.39$nm/\%$ with the transverse-stress compensation. The sensor is very simple and effective, which provides a new method of gas measurement combined with different actual conditions.

INDEX TERMS Methane sensor, transverse-stress compensation, photonic crystal fiber long period grating, surface plasmon resonance.

I. INTRODUCTION

Photonic crystal fiber (PCF) has been widely used in fiber sensing field due to its flexible structure and outstanding optical properties [1]–[5].As a typical mode coupling devices, photonic crystal fiber long-period grating (PCF-LPG) also becomes a research focus. Based on the coupling between core fundamental mode and cladding modes, PCF-LPG has higher sensitivity to the refractive index (RI) change of cladding layer [6]–[8]. By virtue of such characteristic, PCF-LPG is very suitable for measuring different paramet ers [9]–[11]. And then, the demand for real-time remote detection of hazardous-gas in local environment is gradually appearing, especially including the methane monitoring [12]. Therefore, different LPG-based methane sensors are developed to solve this new problem [13], [14]. In 2017, Yang et al. achieved methane detection with a sensitivity of 1.078 $nm/\%$ using a single PCF coated with methane-sensitive film [13]. It verifies the feasibility of the methane measurement via the combined use of methane-sensitive film and PCF-LPG. However, how to make gas-sensitive reaction more adequate is still a problem. So in this paper, we introduce large side-holes into the PCF structure to enhance the reaction efficiency. Obviously, the designed side-hole structure is conducive to film coating and gas diffusion. Since the change in effective refractive index of the cladding is related to the methane concentration, the coupling between core mode LP_{01} and cladding mode LP_{02} would provide higher methane sensitivity.

Meanwhile, the problem is that the side-hole structure is prone to unnecessary deformation when the fiber is under external force. The photo-elastic effect due to transverse-stress also leads to a change in effective refractive index. Hence, it is necessary to take the transverse-stress compensation into account. Based on this concept, we plate the silver nano-film onto the large hole on the right to form a new sensing channel because of SPR effect. The deformation of the silver-plated hole has great influence on the imaginary part of the effective refractive index of core mode. Then, the methane concentration and stress can be demodulated by the

The associate editor coordinating the review of this manuscript and approving it for publication was Paolo Bettini.

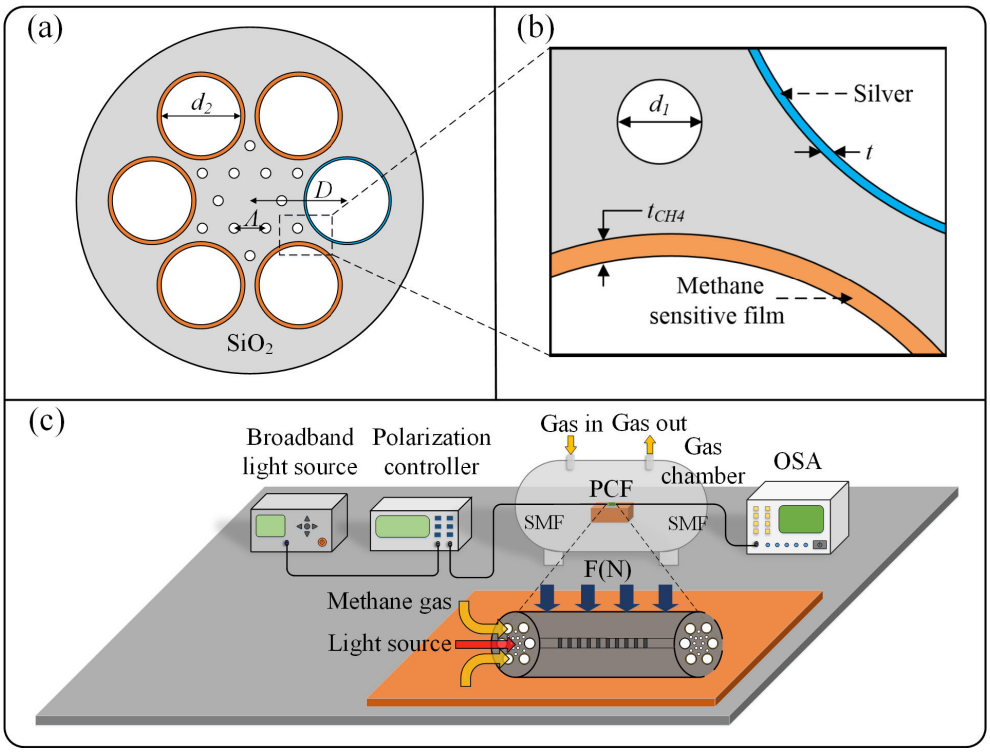

FIGURE 1. (a, b) The cross-section of PCF sensor and (c) principle diagram of the experimental setup.

dual-parameter matrix method [15].The structural parameters are optimized for this purpose, and the working wavelengths of two sensing mechanisms are manipulated to avoid mutual interference. The results show that the device has a high sensitivity of 6.39 $nm/\%$ for methane measurement.

II. MODEL AND METHOD

The cross-section of proposed PCF is shown in Fig.1(a), and six ultra-large holes symmetrically distributed in the outermost layer. The side-hole on the right is plated with silver nano-film having a thickness t when other five holes are coated with methane-sensitive film with the thickness t_{CH4}. Here we select the ultraviolet curable fluoro-siloxane nano-film incorporating cryptophane A as methane-senstive film. Among them, the diameter of smaller hole near the core is d_1, and the diameter of ultra-large hole is d_2. The lattice period is Λ, and the distance between large hole and core is D. We can prepare such PCF through multi-step "stack and draw" procedure [16]. Silica rods and capillaries are stacked together and drawn down by using a standard fiber drawing tower. Fig.1 (c) indicats the experimental setup, and the predetermined methane gas is introduced into the gas chamber to have a free diffusion in the cladding holes. The x-polarization light can be filtered out of the light emmitted from broadband source (BBS) by polarization controller (PC), and then y-polarized light travels to PCF through SMF. Finally, we can obtain responding spectra in optical spectrum analyzer (OSA).

We use the finite element method (FEM) to investigate the spectral characteristic [17]. By discretizing the calculation area, the region is meshed into 58192 domain elements and 3464 boundary elements. The convergence error of the PCF is 10^{-7} found at optical wavelength $\lambda = 1308\ nm$. In addition, we use Sellimeiers equation to describe the dispersion of pure silica which can be seen from (1) [18]. The refractive index of the methane-sensitive film (n_{film}) is linearly dependent on methane concentration (C_{CH4}). According to the experimental results in Ref. [19], the value of n_{film} decreases linearly by 0.0038 for every 1% increase in concentration within the range of 0%-3.5%. Equation (2) shows the relationship between the n_{film} and C_{CH4}, and the reaction is reversible. Since the LPG has high sensitivity to the change of surrounding refractive index (SRI) [7], we can measure the methane concentration C_{CH4} through analyzing the change in n_{film}. PCF-LPG can promote the coupling between the core fundamental mode and co-propagating cladding modes [8], and the coupling should satisfy the phase matching condition shown in (3).

$$n^2 = 1 + \frac{0.6961663\lambda^2}{\lambda^2 - (0.0684043)^2} + \frac{0.4079426\lambda^2}{\lambda^2 - (0.1162414)^2} + \frac{0.8974794\lambda^2}{\lambda^2 - (9.896161)^2} \quad (1)$$

$$n_{film} = 1.4478 - 0.0038C_{CH4} \quad (2)$$

$$\beta_{co} - \beta_{cl} = 2\pi/\Lambda_{LPG} \quad (3)$$

$$\lambda_{res} = \left(n_{eff}^{co} - n_{eff}^{cl}\right)\Lambda_{LPG} \quad (4)$$

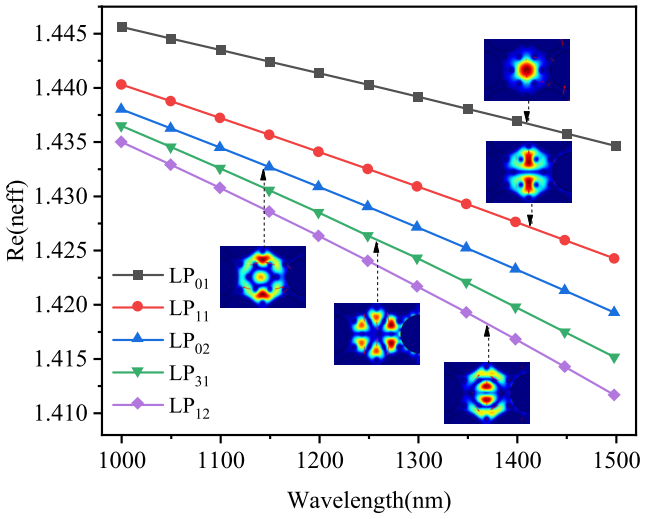

FIGURE 2. The relationship between effective refractive index and wavelength for different modes.

$$\kappa_{co-cl} = \frac{2\pi n \delta_n}{\lambda \sqrt{n_{co}^{eff} n_{cl}^{eff}}} \frac{\iint_{grating-area} E_{co} E_{cl}^{*} dxdy}{\sqrt{\iint_{\infty} |E_{co}|^2 dxdy} \sqrt{\iint_{\infty} |E_{cl}|^2 dxdy}} \tag{5}$$

$$T = 1 - \frac{\sin^2(|\kappa| L \sqrt{1 + (\delta/|\kappa|)^2})}{1 + (\delta/|\kappa|)^2} \tag{6}$$

In (3), β_{co} and β_{cl} are the propagation constants of the core mode and the cladding mode respectively, and Λ_{LPG} represents the period of LPG. Therefore, we can obtain the resonance wavelength of LPG from (4), where n_{eff}^{co} and n_{eff}^{cl} are the effective refractive indices of core mode and the cladding mode, respectively. Fig.2. shows the n_{eff} curves for various modes of proposed PCF structure, and the resonant wavelength decreases with the increase of grating period of proposed PCF-LPG [20]. The coupling coefficient κ of LP_{01}-LP_{02} mode, as shown in (5) [20], [21], where n is the refractive index of silica, δ_n is the index modulation, **E**co and **E**cl are the transverse electric fields of the core mode and the cladding mode, respectively. The LPG transmission coefficient is given by (6). where L is the LPG length, δ is the detuning parameter. Usually, the grating period is set as $100 - 500\mu m$ and the resonant wavelength is chosen in $1300 \sim 1650nm$. In our model, we select grating period $\Lambda_{LPG} = 107\mu$m and the grating length $L_{LPG} = 20mm$. So the modes LP_{01} and LP_{02} can satisfy phase matching condition at $1308nm$, which will lead to a significant drop in corresponding transmission spectrum.

In order to compensate for the stress interference, we coat the silver layer onto the inner surface of right side-hole to form a SPR sensing channel. The dielectric constant of silver can be derived from (7) based on the widely adopted Lorentz-Drude model [22], where $\varepsilon_\infty = 2.48$ is the high frequency dielectric constant, $\omega_p = 1.35 \times 10^{16}\ (rad/s)$ is the plasma frequency and $\omega_d = 7.62 \times 10^{13}\ (rad/s)$ is the damping frequency. As stated in Ref. [22], [23], we can obtain the propagation constant of Surface Plasmon waves (SPWs) k_{SP} from (8), where λ is the wavelength in vacuum, ε_m and ε_d are the permittivity of metal and the material outside the metal respectively. Meanwhile, (9) describes the propagation constant of evanescent wave, where θ is the incident angle of the light wave, $\varepsilon_{co}(\lambda)$ is the dielectric constant of the core. Then, we can calculate the coupling coefficient $\eta(\lambda)$ as (10). In theory, when $\eta(\lambda) = 1$ (i.e. $k_Z = k_{SP}$), the confinement loss of core mode will be reach to maximum [24].

$$\varepsilon(\omega) = \varepsilon_\infty - \frac{\omega_p^2}{\omega(\omega + i\omega_d)} \tag{7}$$

$$k_{SP} = \mathrm{Re}\left(\frac{2\pi}{\lambda}\sqrt{\frac{\varepsilon_d(\lambda)\,\varepsilon_m(\lambda)}{\varepsilon_d(\lambda) + \varepsilon_m(\lambda)}}\right) \tag{8}$$

$$k_Z = \frac{2\pi}{\lambda}\sqrt{\varepsilon_{co}(\lambda)}\sin\theta \tag{9}$$

$$\eta(\lambda) = \frac{|k_Z|}{|k_{SP}|} = \sin\theta\sqrt{\frac{\varepsilon_{co}(\lambda)\,[\varepsilon_d(\lambda) + \varepsilon_m(\lambda)]}{\varepsilon_d(\lambda)\,\varepsilon_m(\lambda)}} \tag{10}$$

That is, the applied stress will cause the change in loss peak spectra, and we can measure the transverse-stress by analyzing the confinement loss peak-shifts of the core mode in y-polarization direction. Compared with x-polarization, y-polarization has more obvious loss peak, which is conducive to spectral detection. The effective refractive index of the core fundamental mode is $n_{eff} = \mathrm{Re}(n_{eff}) + i\mathrm{Im}(n_{eff})$, in which the real part represents the propagation constant of light and the imaginary part relates to the confinement loss [25]. (11) shows the relationship between imaginary part of the effective refractive index and the confinement loss [26].

$$\alpha_{CL}\,(dB/m) = \frac{20}{\ln(10)} \times \frac{2\pi}{\lambda} \times \mathrm{Im}(n_{eff}) \tag{11}$$

Next, we need to optimize the structural parameters for better sensing performance. Then, the gas sensitivity of LPG with different D and t_{CH4} can be obtained as shown in Fig. 3. Fig.4 indicates the variation of the loss spectra of the core fundamental mode in y-polarization direction with different parameters. In other words, we can manipulate the loss peak, resonant wavelength and sensitivity by adjusting such structural parameters. The side-holes should be large enough when the gas sensitivity measured by the LPG is still sufficiently high. In addition, we need to make the loss peak at the communication window of 1550 nm. Therefore, we select the parameters as shown in Table.1 after all these comprehensive considerations. Fig.5 (A) describes the transmission spectrum of PCF-LPG, the coupling between LP_{01} mode and LP_{02} mode happens at around 1308 nm. Fig.5 (B) show the loss spectrum of core fundamental mode in y-polarization direction. The illustrations (a) represent the electric field mode distribution of the LP_{02} mode. (b-d) show the electric field mode distributions of the core mode, the SPP mode, and the resonant coupling, respectively. The coupling between y-polarized core mode and SPP mode occurs at 1570nm.

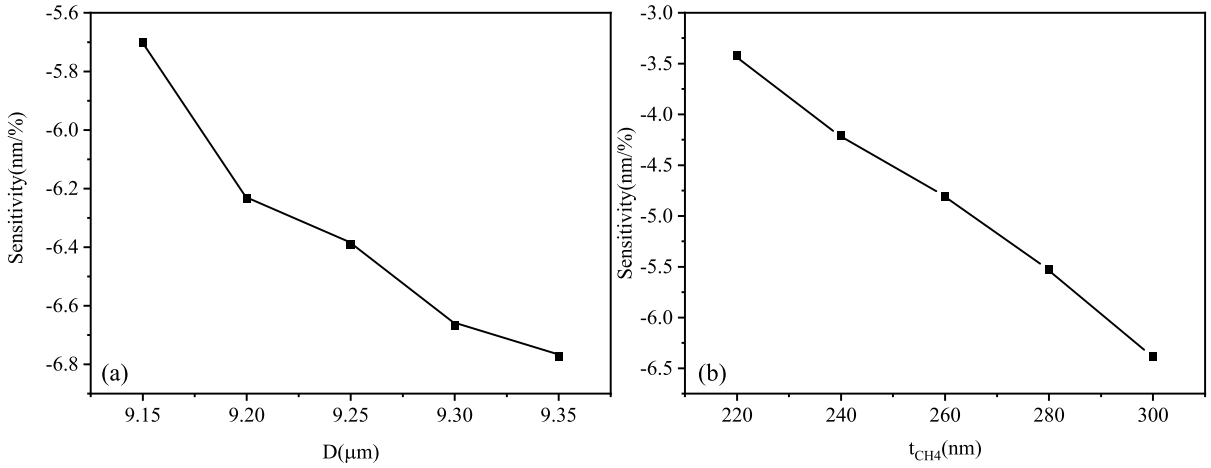

FIGURE 3. Relationship between the gas sensitivity of the sensor and (a) the distance D (b) the thickness t_{CH4}.

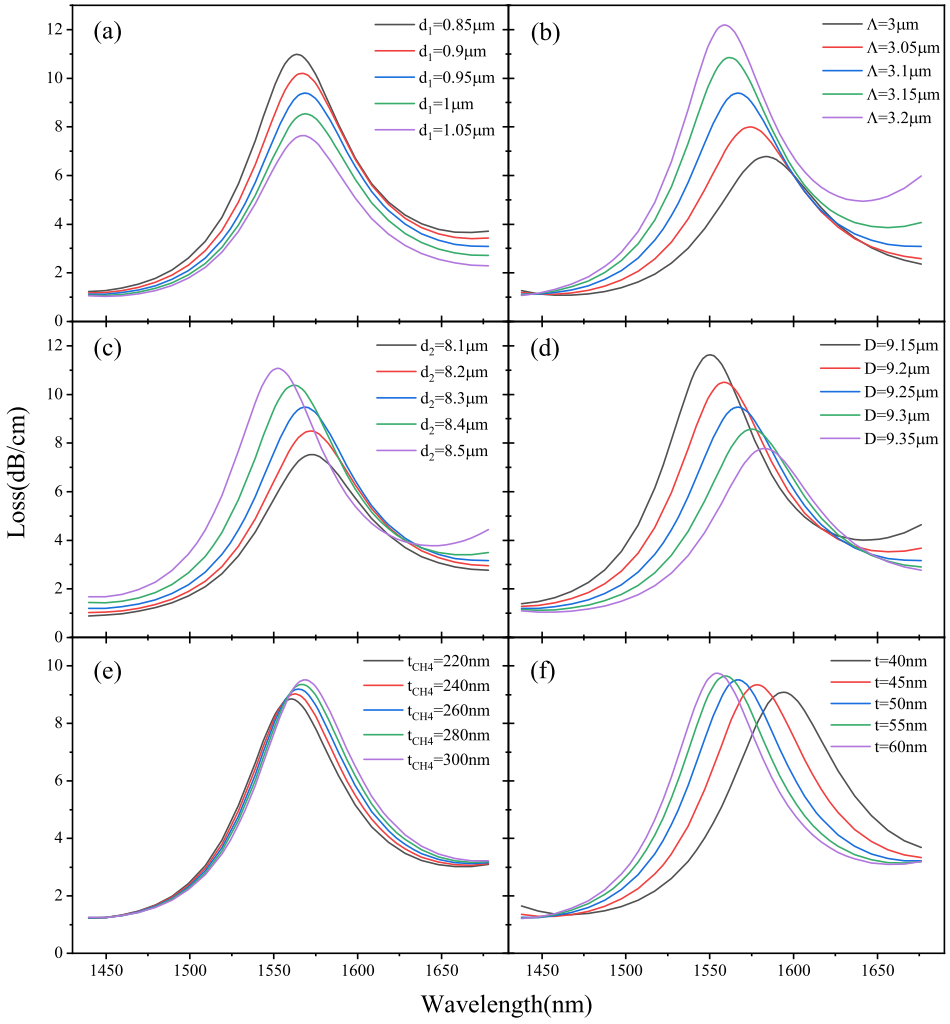

FIGURE 4. The loss peak of y polarized core fundamental mode varies with different values of (a) d_1, (b) Λ, (c) d_2, (d) D, (e) t_{CH4}, (f) t.

In summary, the resonance wavelength of transmission spectrum and loss spectrum will have a peak-shift when the *RI* of methane-sensitive film or transverse stress changes. The sensitivity used in next section can be derived from (12) [27], where $\Delta\lambda_{peak}$ is the wavelength shift (nm) and ΔA represents the variation of gas concentration (percentage)

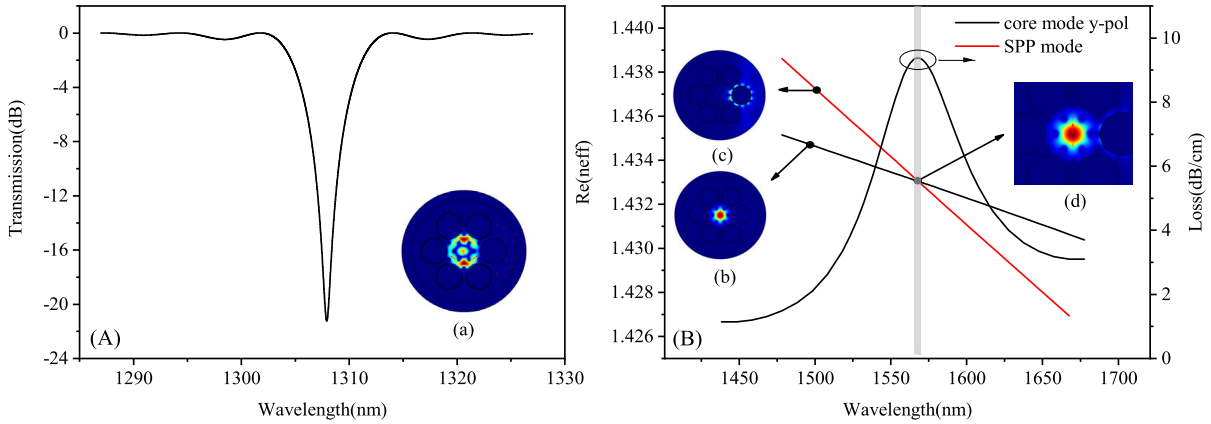

FIGURE 5. (A) The transmission spectrum of LPG, (B) The effective refractive index between the core mode and SPP mode, and the loss spectrum of core fundamental mode in y-polarization direction. The illustrations represent the electric field distribution of (a) LP02 mode, (c) y-polarized core mode, (d) y-polarized SPP mode, (e) the resonance coupling.

TABLE 1. Values of the optimized parameters.

parameter	d_1	Λ	d_2	D	t_{CH4}	t
value (μm)	0.95	3.1	8.3	9.25	0.3	0.05

or transverse-stress (N). Therefore, the units of sensitivity are $nm/\%$ and nm/N, respectively.

$$S = \frac{\Delta\lambda_{peak}}{\Delta A} \tag{12}$$

III. RESULTS AND DISCUSSION

For proposed PCF stucture, the circular hole will be deformed irregularly when the transverse force applied on the fiber. The anisotropic stress distribution would produce elastic-optical effect and change the effective refractive index of different modes [28]. So that we need to consider the geometric deformation and stress distribution of optical fiber under transverse-force firstly. Fig.6 (a) is a schematic illustration of the cross-section under transverse force. In this section, we will apply a uniform force to the PCF within the range of 0-5N. The Young's modulus of silica is $E_{SiO2} = 73.1GPa$ and Poisson's ratio is $v_{SiO2} = 0.17$ [29]. Fig.6 (b) shows the distribution of principal stress components σ_y (in y-direction) when the PCF section is subjected to a transverse-force of $1N$. In order to more clearly show the stress distribution, we select the points on the dotted line in Fig.6 (b) to plot the principal stress components σ_x (in x-direction) and σ_y curves with respect to y-coordinate, as is shown in Fig.7. The negative σ_y indicates that the cross-section is under a downward force, and negative σ_x represents that horizontal compressional stress occurs between large side-holes. Based on photo-elastic effect, (13) describes the relationship between the anisotropic refractive index and stress components [30], where $C_1 = 6.5 \times 10^{-13}\left(m^2/N\right)$ and

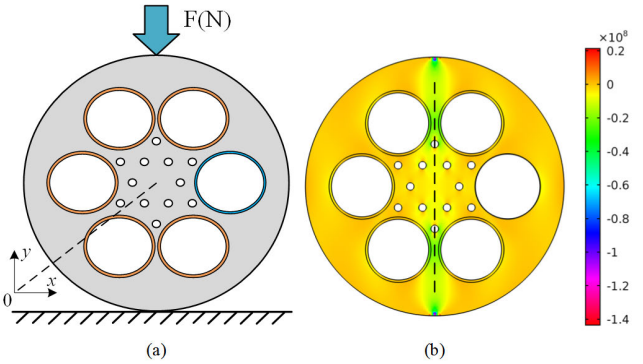

FIGURE 6. (a) Diagram of deformation of PCF under transverse stress, (b) distribution surface of the σ_y $\left(N/m^2\right)$.

$C_2 = 4.2 \times 10^{-12}\left(m^2/N\right)$ are the stress-optic coefficients.

$$\begin{aligned} n_x &= n_0 - C_1\sigma_x - C_2\left(\sigma_y + \sigma_z\right) \\ n_y &= n_0 - C_1\sigma_y - C_2\left(\sigma_x + \sigma_z\right) \end{aligned} \tag{13}$$

Many times, we tend to take into account the elastic-optical effect only, but often ignore the deformation of air holes [29], [31]. However, for proposed side-hole structure, the deformation of large holes has a crucial influence on the propagation of light in the PCF. Therefore, we also need to get the relationship between transverse-stress and geometric deformation.

Figure.8 (a-b) show the displacement field in y-direction and x-direction under $1N$ transverse stress. Then, we can obtain the deformation of the material by applying above displacement components. Since the deformation is difficult to visualize under smaller force, Fig.8 (c-d) indicate the distinct deformation under a transverse stress of $100N$ for a comparison. In Fig.8 (c), the black line denotes the initial geometric frame, and the grey surface represents the deformed material frame. Fig.8 (d) shows the electric field distribution of the fundamental mode at 1585nm under $100N$

TABLE 2. Wavelength-shifts with different conditions (states A, B and C) as an example.

States	Wavelength shift		Actual value	Calculated value	
	$\Delta\lambda_{LPG}(nm)$	$\Delta\lambda_{SPR}(nm)$	$\Delta CH_4(\%)$	ΔCH_4 without F-compensation	ΔCH_4 with F-compensation
A→B	-4.40	-0.59	0.6	0.69	0.62
B→C	-8.02	-0.89	1.2	1.25	1.18
C→A	-12.42	-1.48	1.8	1.95	1.80

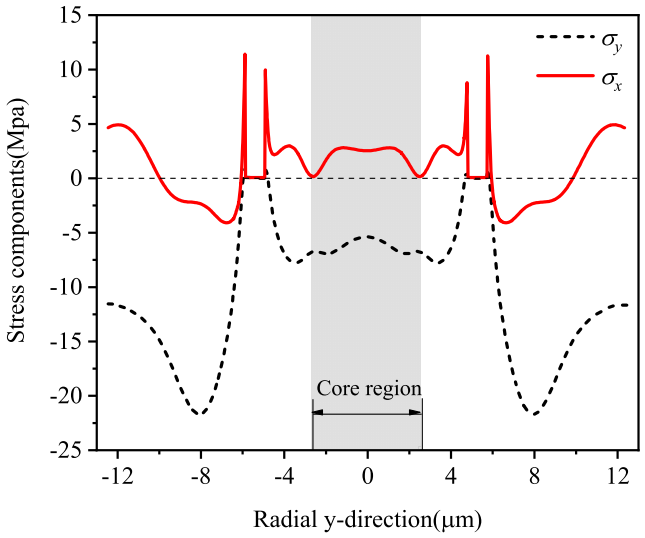

FIGURE 7. The values of σ_X and σ_Y with respect to y-coordinate (Gray area is the core region).

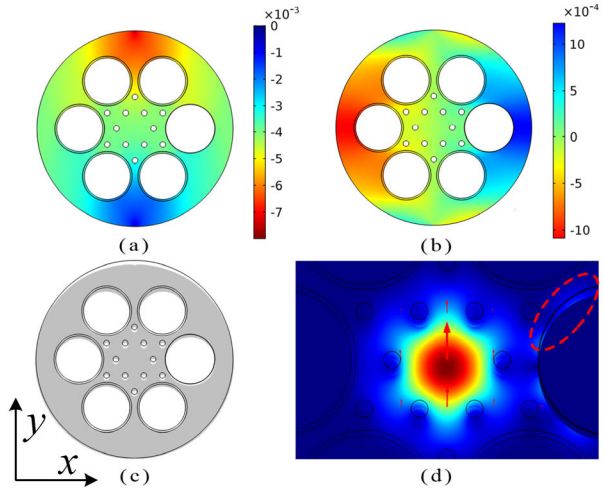

FIGURE 8. (a, b) Displacement field in y-direction and x-directions under 1N transverse stress respectively, (c) Deformation of PCF cross- section, (d) the electric field distribution of core fundamental mode in y-polarization direction under 100N transverse-stress.

transverse stress, and the outline before and after deformation is obvious. Therefore, we can analyze the propagation mode of PCF under different transverse-stresses through

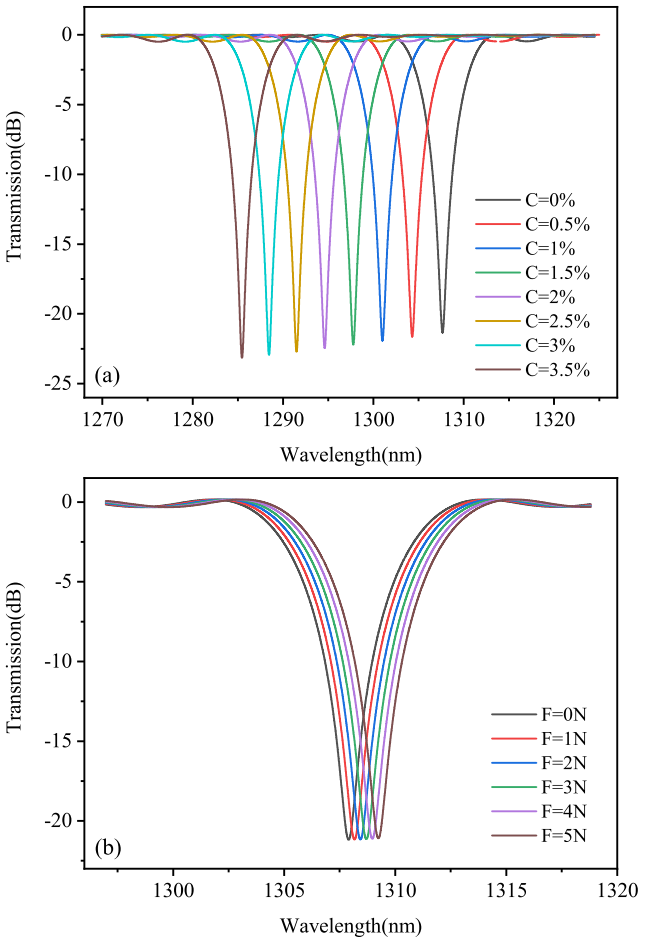

FIGURE 9. Transmission spectra of LPG under different (a) methane concentrations and (b) transverse-stresses.

this improved method. That is the basis of the research on proposed PCF-LPG methane sensor. After considering the explosion limit of methane gas and the linear demodulation requirement [19], we only measure methane gas within the concentration range of 0-3.5%.

Fig.9 (a) is the transmission spectra of LPG under different methane concentrations when $F = 0N$. The spectral peak shifts toward short wavelength with the increase of concentration. Meanwhile, Fig.9 (b) shows the transmission spectral peak-shifts under different transverse stresses in the absence of methane gas. Similarly, Fig.10 (a-b) indicates the loss

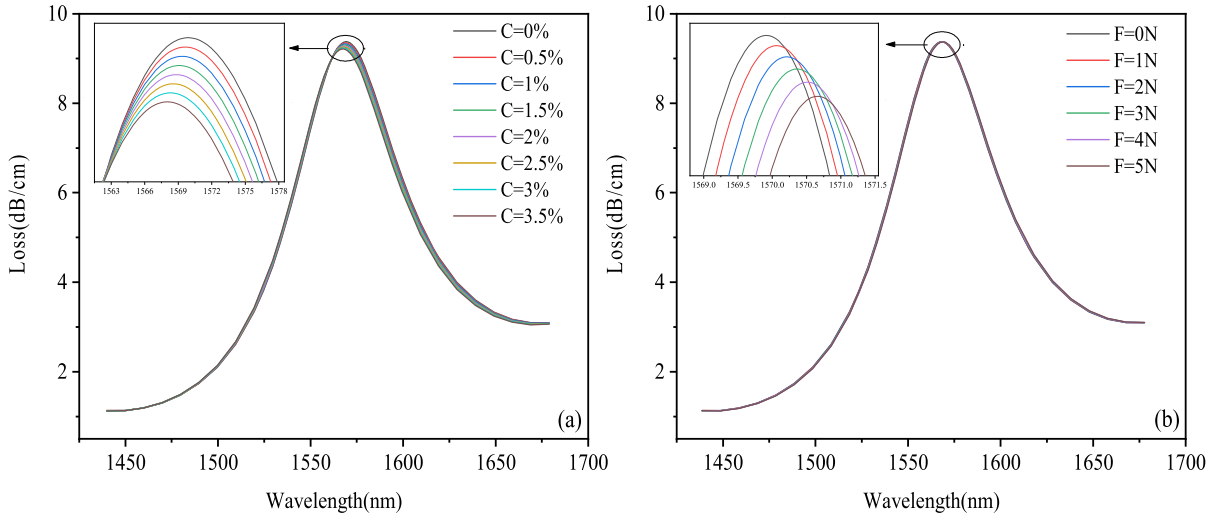

FIGURE 10. Loss spectra of core mode under different (a) methane concentrations and (b) transverse-stresses.

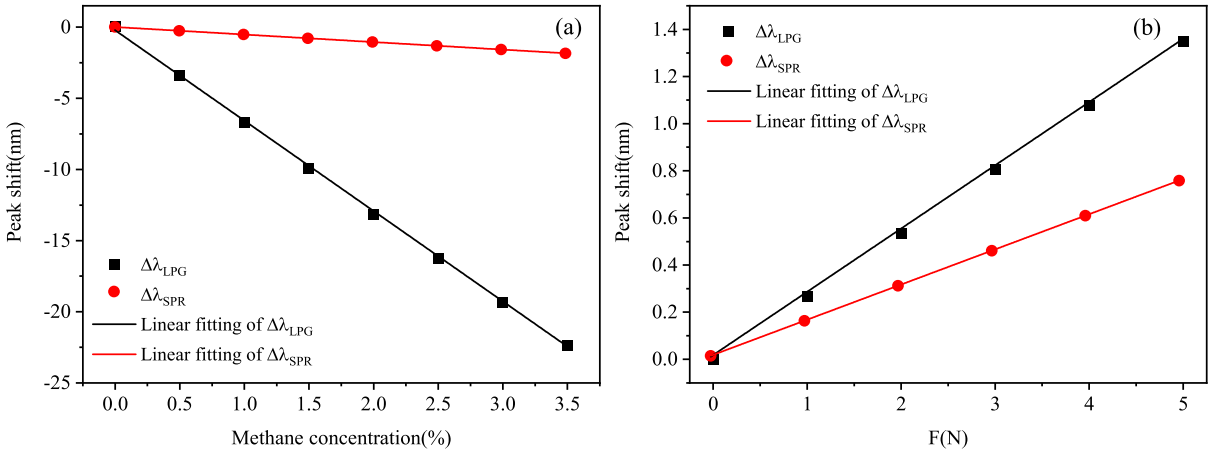

FIGURE 11. The resonant wavelength-shift for different (a) methane concentrations and (b) transverse forces.

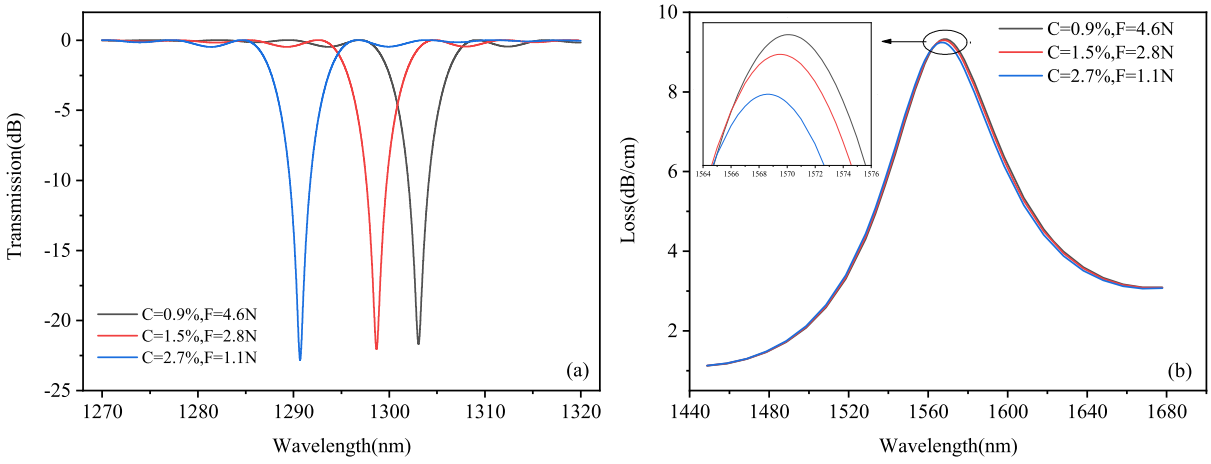

FIGURE 12. (a) The transmission spectrum and (b) loss spectrum under three different conditions.

spectra of *y*-polarized core fundamental mode under different concentrations and transverse stresses, respectively. Then, Fig.11 describes the sensitivity coefficients of LPG and SPR sensing channels directly. Through (14), methane concentration (ΔCH_4) and transverse stress (ΔF) can be calculated out by measuring the resonant wavelength-shifts, and the

values of coefficients matrix elements are $k_1 = -6.39nm/\%$, $k_2 = 0.27nm/N$, $k_3 = -0.53nm/\%$, $k_4 = 0.15nm/N$.

$$\begin{bmatrix} \Delta\lambda_{LPG} \\ \Delta\lambda_{SPR} \end{bmatrix} = \begin{bmatrix} k_1 & k_2 \\ k_3 & k_4 \end{bmatrix} \begin{bmatrix} \Delta CH_4 \\ \Delta F \end{bmatrix} \tag{14}$$

Since the external environment often changes randomly during the sensing process, we define a two-dimensional parameter ($CH4$ (%), F (N)) to match the actual situation. Three random sampling points including A (0.9%, 4.6N), B (1.5%, 2.8N) and C (2.7%, 1.1N) are selected as an example. The actual values of the methane concentration change come from the selected sampling points. Fig. 12 (a) and (b) show the transmission and loss spectra of the PCF under the corresponding conditions, respectively. Table 2 shows the shifts of the resonance wavelength under above three conditions, and the calculation results show that they are consistent with the actual situation. Obviously, the measurement accuracy is higher when the transverse-stress compensation is considered.

IV. CONCLUSION

In conclusion, we designed a new PCF-LPG methane sensor considering transverse-stress compensation, and the methane sensitivity can reach up to 6.39 $nm/\%$. The application of side-hole structure makes it easier to coat methane-sensitive film onto the inner surface of holes. Especially, the large holes are conducive to the rapid diffusion and fully reaction of methane gas. After comprehensive consideration of photoelastic effect and material deformation caused by transverse-stress, we can achieve high sensitivity and accuracy of methane measurement

ACKNOWLEDGMENT

Thanks to the modern analysis and computing center of CUMT for providing COMSOL software.

REFERENCES

[1] J. C. Knight, T. A. Birks, P. St. J. Russell, and D. M. Atkin, "All-silica single-mode optical fiber with photonic crystal cladding," *Opt. Lett.*, vol. 21, no. 19, pp. 1547–1549, 1996, doi: 10.1364/ol.22.000484.

[2] O. Frazao, J. L. Santos, and F. M. Araujo, "Optical sensing with photonic crystal fibers," *Laser Photon. Rev.*, vol. 6, no. 2, pp. 449–459 Nov. 2008, doi: 10.1002/lpor.200810034.

[3] T. A. Birks, J. C. Knight, and P. S. J. Russell, "Endlessly single-mode photonic crystal fiber," *Opt. Lett.*, vol. 22, no. 13, pp. 961–963, Jul. 1997, doi: 10.1364/OL.22.000961.

[4] Q. Liu, S.-G. Li, and X. Wang, "Sensing characteristics of a MF-filled photonic crystal fiber Sagnac interferometer for magnetic field detecting," *Sens. Actuators B, Chem.*, vol. 242, pp. 949–955, Apr. 2017, doi: 10.1016/j.snb.2016.09.160.

[5] Q. Liu, S. Li, H. Chen, Z. Fan, and J. Li, "Photonic crystal fiber temperature sensor based on coupling between liquid-core mode and defect mode," *IEEE Photon. J.*, vol. 7, no. 2, Apr. 2015, Art. no. 4500509, doi: 10.1109/JPHOT.2015.2404911.

[6] Z. He, Y. Zhu, and H. Du, "Long-period gratings inscribed in air-and water-filled photonic crystal fiber for refractometric sensing of aqueous solution," *Appl. Phys. Lett.*, vol. 92, no. 4, p. 1193, Jan. 2008, doi: 10.1063/1.2838349.

[7] A. Maity and S. K. Varshney, "Ultrasensitive properties of a long-period grating inscribed in a dual-mode photonic crystal fiber," *IEEE Sensors J.*, vol. 14, no. 8, pp. 2833–2840, Aug. 2014, doi: 10.1109/jsen.2014.2317877.

[8] L. Rindorf and O. Bang, "Highly sensitive refractometer with a photonic-crystal-fiber long-period grating," *Opt. Lett.*, vol. 33, no. 6, pp. 563–565, Mar. 2008, doi: 10.1364/OL.33.000563.

[9] X. Zhong, Y. Wang, C. Liao, S. Liu, J. Tang, and Q. Wang, "Temperature-insensitivity gas pressure sensor based on inflated long period fiber grating inscribed in photonic crystal fiber," *Opt. Lett.*, vol. 40, no. 8, pp. 1791–1794, Apr. 2015, doi: 10.1364/OL.40.001791.

[10] Y. Zhu, Z. He, J. Kaňka, and H. Du, "Numerical analysis of refractive index sensitivity of long-period gratings in photonic crystal fiber," *Sens. Actuators B, Chem.*, vol. 129, no. 1, pp. 99–105, Jan. 2008, doi: 10.1016/j.snb.2007.07.117.

[11] L. H. Rindorf, J. B. Jensen, and M. Dufva, "Photonic crystal fiber long-period gratings for biochemical sensing," *Opt. Express*, vol. 14, no. 18, pp. 8224–8231, Jul. 2006, doi: 10.1364/OE.14.008224.

[12] S. Kundu, J. Zanganeh, and B. Moghtaderi, "A review on understanding explosions from methane-air mixture," *J. Loss Prevention Process Ind.*, vol. 40, pp. 507–523, Feb. 2016, doi: 10.1016/j.jlp.2016.02.004.

[13] J. Yang, X. Che, and R. Shen, "High-sensitivity photonic crystal fiber long-period grating methane sensor with cryptophane-A-6Me absorbed on a PAA-CNTs/PAH nanofilm," *Opt. Express*, vol. 25, no. 17, pp. 20258–20267, Jul./Aug. 2017, doi: 10.1364/OE.25.020258.

[14] J. Yang, L. Zhou, and J. Huang, "Sensitivity enhancing of transition mode long-period fiber grating as methane sensor using high refractive index polycarbonate/cryptophane A overlay deposition," *Sens. Actuators B, Chem.*, vol. 207, pp. 477–480, Oct. 2015, doi: 10.1016/j.snb.2014.10.013.

[15] S. Liu, W. Zhe, and M. Hou, "Asymmetrically infiltrated twin core photonic crystal fiber for dual-parameter sensing," *Opt. Laser Technol.*, vol. 82, pp. 53–56, Feb. 2016, doi: 10.1016/j.optlastec.2016.02.014.

[16] J. Ma, H. Yu, and X. Jiang, "High-performance temperature sensing using a selectively filled solid-core photonic crystal fiber with a central air-bore," *Opt. Express*, vol. 25, no. 8, pp. 9406–9415, Apr. 2017, doi: 10.1364/OE.25.009406.

[17] K. Saitoh and M. Koshiba, "Full-vectorial imaginary-distance beam propagation method based on a finite element scheme: Application to photonic crystal fibers," *IEEE J. Quantum Electron.*, vol. 38, no. 7, pp. 927–933, Jul. 2002, doi: 10.1109/JQE.2002.1017609.

[18] E. K. Akowuah, T. Gorman, H. Ademgil, S. Haxha, G. K. Robinson, and J. V. Oliver, "Numerical analysis of a photonic crystal fiber for biosensing applications," *IEEE J. Quantum Electron.*, vol. 48, no. 11, pp. 1403–1410, Nov. 2012, doi: 10.1109/JQE.2012.2213803.

[19] J. Yang, L. Zhou, and X. Che, "Photonic crystal fiber methane sensor based on modal interference with an ultraviolet curable fluoro-siloxane nano-film incorporating cryptophane A," *Sens. Actuators B, Chem.*, vol. 235, pp. 717–722, May 2016, doi: 10.1016/j.snb.2016.05.125.

[20] W. Zhi, J. Jian, and W. Jin, "Scaling property and multi-resonance of PCF-based long period gratings," *Opt. Express*, vol. 12, no. 25, pp. 6252–6257, Nov. 2004, doi: 10.1364/OPEX.12.006252.

[21] J. Kanka, "Design of turn-around-point long-period gratings in a photonic crystal fiber for refractometry of gases," *Sens. Actuators B, Chem.*, vol. 182, pp. 16–24, Feb. 2013, doi: 10.1016/j.snb.2013.02.048.

[22] B. Lee, S. Roh, and J. Park, "Current status of micro- and nano-structured optical fiber sensors," *Opt. Fiber Technol.*, vol. 15, no. 3, pp. 209–221, 2009, doi: 10.1016/j.yofte.2009.02.006.

[23] Y. Wang, Q. Huang, and W. Zhu, "Novel optical fiber SPR temperature sensor based on MMF-PCF-MMF structure and gold PDMS film," *Opt. Express*, vol. 27, no. 8, p. 10813, Jan. 2018, doi: 10.1364/OE.26.001910.

[24] L. Duan, X. Yang, and Y. Lu, "Hollow-fiber-based surface plasmon resonance sensor with large refractive index detection range and high linearity," *Appl. Opt.*, vol. 56, no. 36, pp. 9907–9912, Dec. 2017, doi: 10.1364/AO.56.009907.

[25] X. Yu, S. Zhang, and Y. Zhang, "An efficient approach for investigating surface plasmon resonance in asymmetric optical fibers based on birefringence analysis," *Opt. Express*, vol. 18, no. 17, pp. 17950–17957, Aug. 2010, doi: 10.1364/OE.18.017950.

[26] F. Wang, Z. Sun, and C. Liu, "A highly sensitive dual-core photonic crystal fiber based on a surface plasmon resonance biosensor with silver-graphene layer," *Plasmonics*, vol. 12, no. 6, pp. 1847–1853, Dec. 2017, doi: 10.1007/s11468-016-0453-5.

[27] Q. Liu, B. Yan, and J. Liu, "U-shaped photonic quasi-crystal fiber sensor with high sensitivity based on surface plasmon resonance," *Appl. Phys. Express*, vol. 12, no. 5, Apr. 2019, Art. no. 052014, doi: 10.7567/1882-0786/ab13bc.

[28] C. Wu, J. Li, and X. Feng, "Side-hole photonic crystal fiber with ultra-high polarimetric pressure sensitivity," *J. Lightw. Technol.*, vol. 29, no. 7, pp. 943–948, Apr. 1, 2011, doi: 10.1109/JLT.2011.2109370.
[29] G. Hu and D. Chen, "Side-hole dual-core photonic crystal fiber for hydrostatic pressure sensing," *J. Lightw. Technol.*, vol. 30, no. 14, pp. 2382–2387, Jul. 15, 2012, doi: 10.1109/JLT.2012.2198615.
[30] F. C. Fávero, S. M. M. Quintero, and C. Martelli *et al.*, "Hydrostatic pressure sensing with high birefringence photonic crystal fibers," *Sensors*, vol. 10, no. 11, pp. 9698–9711, Nov. 2010, doi: 10.3390/s101109698.
[31] D. Chen, G. Hu, M.-L. V. Tse, and H. Y. Tam, "Dual-core side-hole fiber for pressure sensing based on intensity detection," *J. Electromagn. Waves Appl.*, vol. 25, nos. 5–6, pp. 775–784, 2011, 10.1163/156939311794827140.

HAI LIU received the B.S. and M.S. degrees in optical engineering from the Huazhong University of Science and Technology, in 2003 and 2006, respectively, and the Ph.D. degree in physical electronics from the Wuhan National Laboratory for Optoelectronics, in 2009. He is currently an Associate Professor with the China University of Mining and Technology. His current research interests include integrated optoelectronic, computational electromagnetic, and photonics.

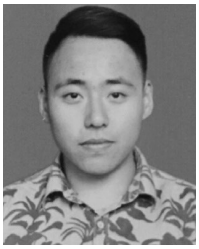

YANZENG ZHANG received the bachelor's degree in automation from the Shenyang University of Technology, China, in 2017. He is currently pursuing the master's degree with the China University of Mining and Technology. His current research focuses on the photonic crystal fiber sensing and photonic crystal waveguide sensing.

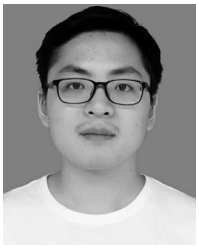

CONG CHEN received the bachelor's degree in electronic communication engineering from the Harbin University of Science and Technology, China, in 2018. He is currently pursuing the master's degree with the China University of Mining and Technology. His major research focuses on nanometer metal array gas sensing.

BINGBING BAI received the bachelor's degree in new energy science and engineering from the Changshu Institute of Technology, China, in 2017. He is currently pursuing the master's degree with the China University of Mining and Technology. His major research focuses on photonic crystal fiber sensing.

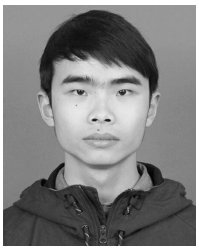

QIYUAN SHAO received the bachelor's degree from Hefei Normal University, China, in 2017. He is currently pursuing the master's degree with the China University of Mining and Technology. His major research focuses on photonic crystal waveguide.

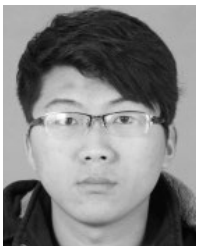

HAORAN WANG received the bachelor's degree in Internet of Things engineering from the Nanyang Institute of Technology, China, in 2017. He is currently pursuing the master's degree with the China University of Mining and Technology. His current research focuses on the photonic crystal fiber sensing and photonic crystal waveguide sensing.

WEN ZHANG received the bachelor's degree in electronic science and technology from the Fuyang Teachers College, China, in 2017. She is currently pursuing the master's degree with the China University of Mining and Technology. Her major research focuses on photonic crystal fiber gas sensing.

CANCAN CHEN received the bachelor's degree in photoelectric information science and engineering from Shandong Jianzhu University, China, in 2017. She is currently pursuing the master's degree with the China University of Mining and Technology. Her major research focuses on dual-core photonic crystal fiber plasmonic refractive index sensor.

SHOUFENG TANG received the B.S. degree in physics from Northeast Normal University, in 1992, the M.S. degree in measurement technology and instrument from the Nanjing University of Aeronautics and Astronautics, in 2005, and the Ph.D. degree in testing technology and automation device from the China University of Mining and Technology, in 2011. He is currently a Professor with the China University of Mining and Technology. His current research interests include detection technology, automation device, and sensor technology.